Check for updates

Received: 20 September 2021 | Revised: 6 January 2022 | Accepted: 8 January 2022

DOI: 10.1002/suco.202100655

ARTICLE

fib CEB-FIP WILEY

Experimental tests on shallow foundations of onshore wind turbine towers

Bruno Dal Lago[1] | **Luca Flessati**[2] | **Pietro Marveggio**[2] | **Paolo Martinelli**[2] | **Giancarlo Fraraccio**[3] | **Claudio di Prisco**[2] | **Marco di Prisco**[2]

[1]Department of Theoretical and Applied Sciences, Università degli Studi dell'Insubria, Varese, Italy

[2]Department of Civil and Environmental Engineering, Politecnico di Milano, Milan, Italy

[3]Enel Green Power, Engineering and Construction Unit, Rome, Italy

Correspondence
Bruno Dal Lago, Department of Theoretical and Applied Sciences, Università degli Studi dell'Insubria, via Dunant, 3, 21100, Varese, Italy.
Email: bruno.dallago@uninsubria.it

Funding information
Enel Green Power S.p.a.

Abstract

The current effort towards the progressive switch from carbon-based to renewable energy production is leading to a relevant spreading of both on- and offshore wind turbine towers. Regarding reinforced concrete shallow foundations of onshore wind turbine steel towers, possible reductions of reinforcement may increase their sustainability, speed of erection, and competitiveness. The article presents the results of an experimental program carried out at Politecnico di Milano concerning both cyclic and monotonic loading, simulating extreme wind conditions on 1:15 scaled models of wind turbine steel towers connected by stud bolt adapters to reinforced concrete shallow foundations embedded in a sandy soil. Three couples of foundation specimens were tested with different reinforcement layouts: (a) similar to current praxis, (b) without shear reinforcement, and (c) without shear reinforcement and with 50% of ordinary steel rebars replaced by steel fibers. Additional vertical loads were added to the small-scale models in order to ensure similarity in terms of stresses. The test results allowed to (i) characterize the mechanical behavior of the foundation element considering soil-structure interaction under both service and ultimate load conditions, (ii) assess the foundation failure mode, (iii) highlight the role of each typology of reinforcing bars forming the cage, and (iv) provide hints for the optimization of these latter.

KEYWORDS

fiber-reinforced concrete, experimental testing, granular material, reinforced concrete, shallow foundations, soil–structure interaction, wind turbine towers

1 | INTRODUCTION

The increasing demand for green energy production throughout the world fosters the spreading of both on-

Discussion on this paper must be submitted within two months of the print publication. The discussion will then be published in print, along with the authors' closure, if any, approximately nine months after the print publication.

This is an open access article under the terms of the Creative Commons Attribution-NonCommercial-NoDerivs License, which permits use and distribution in any medium, provided the original work is properly cited, the use is non-commercial and no modifications or adaptations are made.
© 2022 The Authors. *Structural Concrete* published by John Wiley & Sons Ltd on behalf of International Federation for Structural Concrete.

and off-shore wind turbines and farms. As a matter of fact, their diffusion involves several multi-disciplinary challenges for the Engineering community,[1] related to the growing demand for higher towers carrying larger rotors having recently overcome 160 m diameter.[2] Higher tower heights are associated with significantly larger actions on the system, implying an increase in complexity in both mechanical and structural design. For an optimized structural design of the towers,[3,4] crucial becomes the study of the foundation system, despite statistically only a minor number of reported collapse cases was associated to inadequacy of foundations.[5,6] Especially referring to wind turbines with steel mast, their foundation system has to sustain cyclically applied large horizontal forces and overturning moments induced by wind load with contemporary moderate vertical load. Two types of foundation systems are mostly employed for onshore towers[7,8]: truncated-conical shallow foundations,[9,10] eventually combined with piles,[11] or deep monopiles,[12] being the former one the most common solution. The connection of the steel mast of tubular towers with the reinforced concrete foundation is usually bolted, where either large steel rings or stud bolt adapters are alternatively employed.[13] Shallow foundations are usually reinforced by (i) radial and circumferential top and bottom rebar layers resisting longitudinal and transverse bending moments, (ii) tall stirrups resisting shear, (iii) additional rebars resisting local bursting and punching actions and (iv) top and bottom meshes allowing for splicing of the radial reinforcement. The reinforcing cage is massive (Figure 1), with subsequent important labor, time, and economic effort. Thus, its optimization may increase the competitiveness of wind farms with respect to different energy production plants. The design of the cage is often driven by code limitations for minimum reinforcement ratios (for both shear and bending reinforcement). These limitations, originally conceived for standard structures, are not tailored for massive structures, such as the foundation elements of wind towers. A proper foundation structural design, avoiding development of both radial and circumferential cracks,[14–23] significantly reduces maintenance costs and extends wind tower lifecycle. The dynamics of the towers is strongly influenced by Soil-Structure Interaction (SSI) under lateral loads,[24–28] eventually including seismic actions,[29–33] although the relative lightness of either tubular or lattice steel towers makes their seismic performance often not critical with respect to the predominant action induced by wind. Corrective actions to an unproper structural design of the foundation system are possible, although complex and invasive.[34,35]

In the framework of a wider experimental/numerical research program,[36–38] in this article the authors present the results of a series of quasi-static cyclic and monotonic experimental tests carried out on 1:15 scaled specimens of wind turbine towers, founded on reinforced concrete circular shallow footings positioned over granular soil strata.

This experimental activity was aimed at characterizing the mechanical behavior of the system under: (i) vertical loads associated with the structure self-weight, (ii) wind-induced cyclic service loads, and (iii) wind-induced ultimate loads. Failure mechanisms of combined tower and foundation system are addressed from both a global (load–displacement and moment-rotation curves) and a local perspective (cracks development and reinforcement yielding), allowing to highlight the safety margins associated with the current typical design approach regarding both shear and bending reinforcements. Moreover, the reliability of alternative reinforcement layouts and solutions was also experimentally addressed. In particular, two strategies were envisaged for optimizing the reinforcing cage: (i) the removal of all vertical tall stirrups, including those placed for shear reinforcement out of the central area of the mast and those placed in correspondence of the rings for load distribution and (ii) the stirrup removal along with the replacement of 50% of both radial and circumferential rebars with metallic fibers dispersed in the concrete matrix. Both strategies may lead to relevant saving of material consumption and, especially the latter solution, of assemblage time and labor.

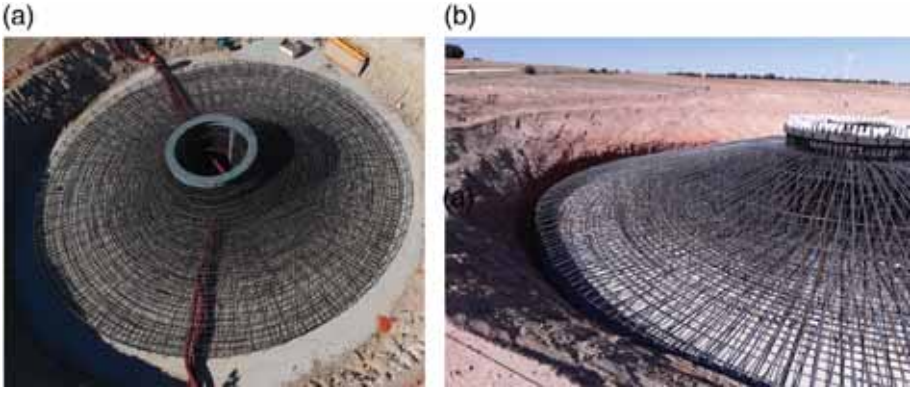

FIGURE 1 Typical reinforcement cages of reinforced concrete shallow foundations for onshore wind turbine towers: (a) top view and (b) side view

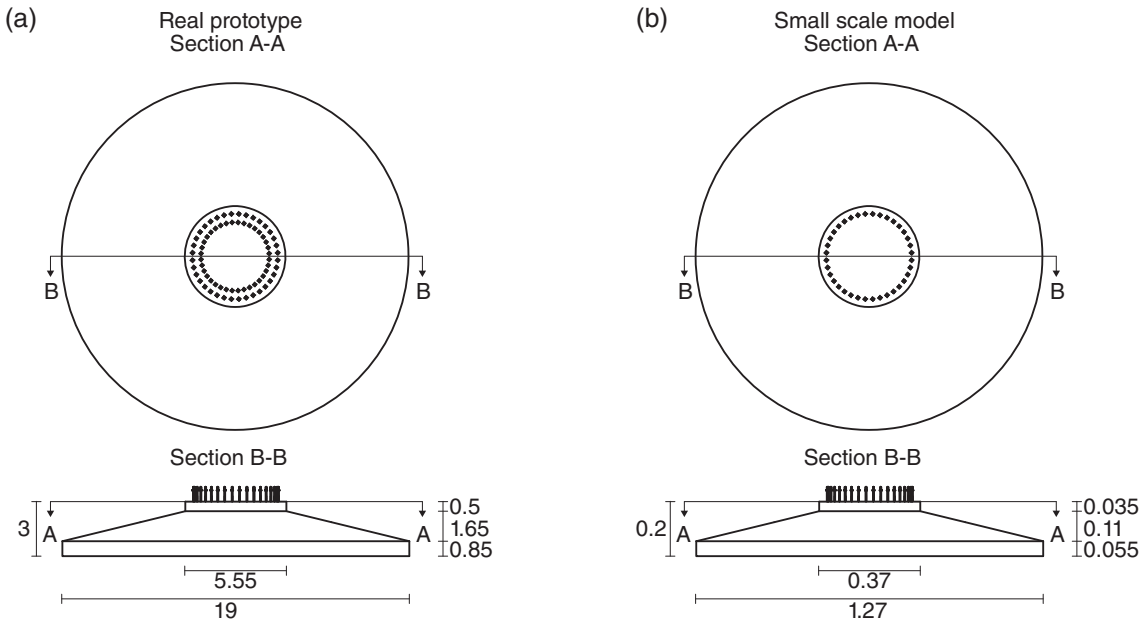

FIGURE 2 Geometry of (a) real prototype and (b) scaled foundation specimens (units: m)

The experimental results are instrumental for both tuning simplified design approaches and calibrating/validating numerical models able to investigate further loading situations, reinforcement solutions and soil conditions, which are however not tackled in the present article.

2 | EXPERIMENTAL PROGRAM

The experimental tests, carried out at the Laboratory of Material, Structure and Construction Testing (LPMSC) of Politecnico di Milano in its large testing facility (GIMED), were performed on small-scale models reproducing real scale 85 m-tall wind turbine towers supporting 3.5 MW aerogenerators founded on truncated-conical shallow footings with a diameter of 19 m (Figure 2a). The connection between tower and foundation is ensured by posttensioned high-strength threaded studs.

In order to properly simulate the real behavior of the soil-foundation-tower assembly under horizontal loads, while finding the best compromise to fit the specimen in the laboratory facility, models geometrically scaled down by a factor $\lambda = 15$ were built and tested (Figure 2b). Balancing the needs to minimize the distortion from the full similitude according to the Theory of Models,[39] and to employ traditional materials which could simulate the nonlinear behavior of the equivalent full-scale ones under the complex multi-axial stress history induced by the test sequence, (i) concrete was cast by employing aggregates with maximum diameter of 12 mm; (ii) steel reinforcing bars had 5 mm diameter; and (iii) metallic fibers, where employed, had diameter of 0.16 mm. The

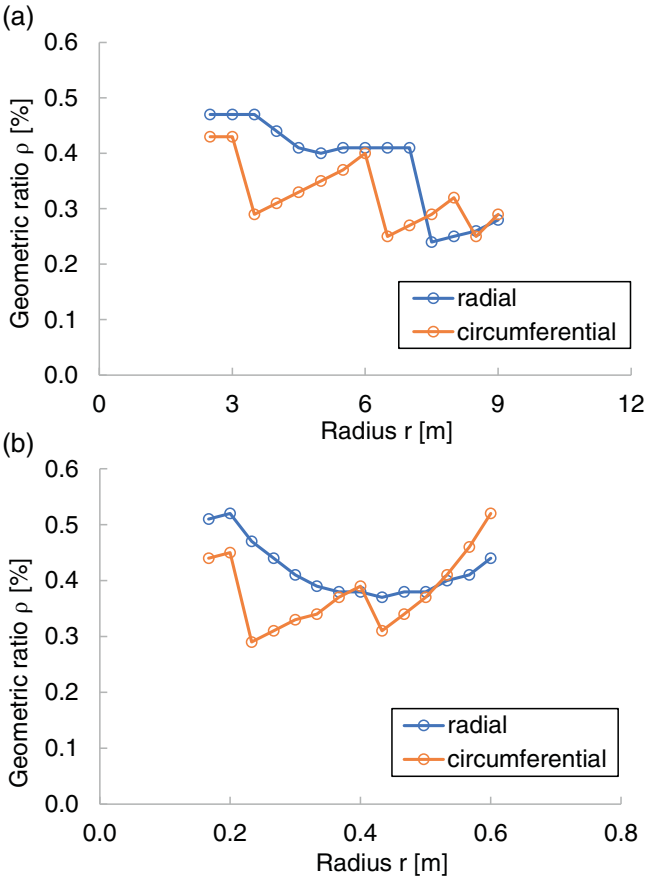

FIGURE 3 Geometric reinforcement ratio of (a) real prototype and (b) scaled model of foundation

reinforcement cage of the small-scale model foundation was arranged to attain geometric reinforcement ratios similar to the real prototype, as shown in Figure 3. Unavoidable small deviations were introduced due to the discretization of the reinforcement cage.

The loading system was designed on the basis of one predefined wind-induced Ultimate Limit State (ULS) Design Load Condition (DLC), selected among the most severe of a typical set. The load values associated with the considered DLC are listed in Table 1. In the prototype, the ratio of base overturning moment M (at the mast-foundation interface) and base horizontal shear load H at ULS (M_{ULS}/H_{ULS}) is equal to 74 m (considering wind load acting on both aerogenerator and mast). Scaled down, it becomes 74 / 15 = 4.93 m. The point of application of the concentrated horizontal force in the test was placed at this height from the base of the small-scale model mast. The operation of geometrical scaling is associated with a reduction in vertical stresses associated with gravity load (λ times lower than in the real prototype). Additional masses were then designed and installed to ensure similarity in terms of vertical stresses.

TABLE 1 Design loads and scaling strategy

	M_{ULS} kNm	H_{ULS} kN	M_{ULS}/H_{ULS} m	V_{ULS} kN
Real prototype	81,450	1100	74.0	21,320
Scaled model	24.1	4.9	4.9	94.8
Scaling factor (λ)	λ^3	λ^2	λ	λ^2

2.1 | Small-scale model description

As previously mentioned, the foundation specimens, geometrically scaled by λ (geometry shown in Figure 2b), had a diameter D = 1.27 m. Six foundations, made by three couples of nominally identical specimens, were manufactured in a precast concrete plant (Figure 4): (i) the real prototype foundation is reproduced by the model specimens FO1-1 and FO1-2 (the reinforcement cage layout is represented in Figure 5); (ii) all stirrups were removed in FO2-1 and FO2-2; (iii) all stirrups and 50% both radial and circumferential reinforcements were replaced by metallic fibers dispersed in the concrete matrix in FO3-1 and FO3-2.

The foundation, embedded at a scaled depth of 0.185 m from the ground surface, was positioned on a 1.5 m thick dry sand stratum. The employed granular material, fine Ticino sand with a grain diameter ranging in between 0.1~1.0 mm, was contained in a 3.64 m diameter cylindric pool. The overall pool sizes were chosen after a series of ad hoc preliminary numerical analyses, whose results (not reported for the sake of brevity) showed that this geometry, under the considered loading conditions, is not affected by boundaries, due to the high localization of the stress in the soil associated to the predominant bending component of the load applied.

The tower mast is a steel pipe with a welded flange base ring. Its external diameter (273 mm) is approximately λ times smaller than the real one (4 m) whereas its thickness (20 mm) is about seven times larger with respect to the theoretical scaled value. This choice is justified by the

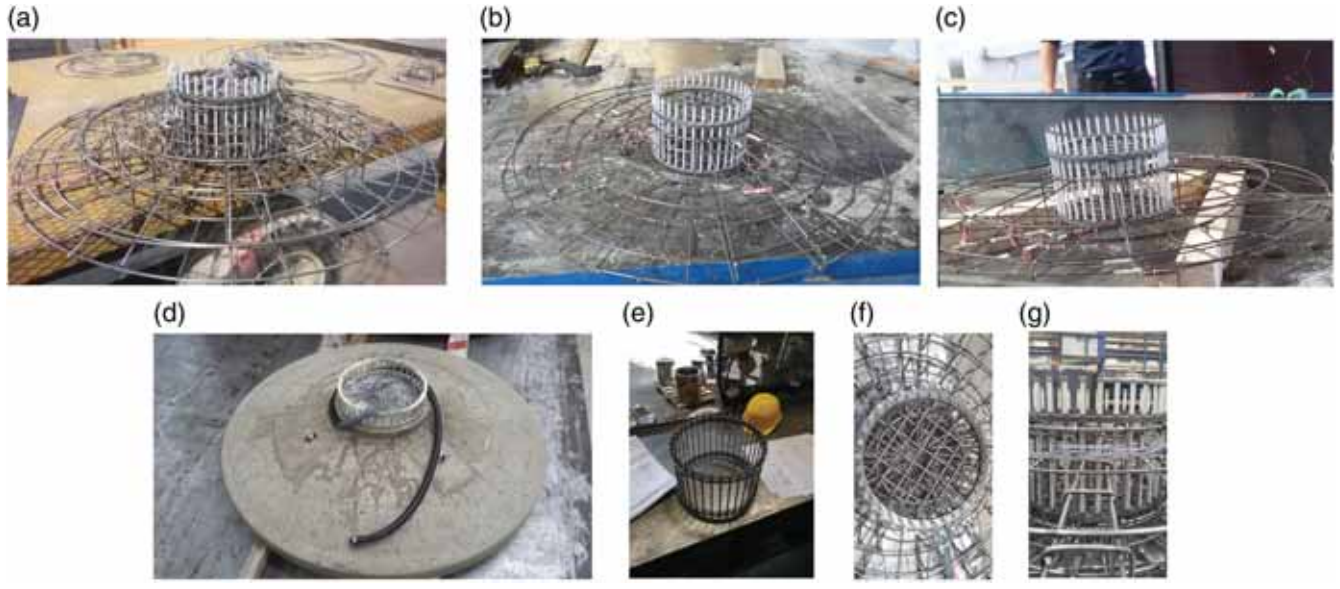

FIGURE 4 Fabrication process of foundation specimens: (a) FO1 assembled cage; (b) FO2 assembled cage; (c) FO3 assembled cage; (d) FO1-1 specimen after demoulding; (e) unbonded posttensioning cage; (f) top detail of FO1 cage; and (g) side detail of FO1 cage

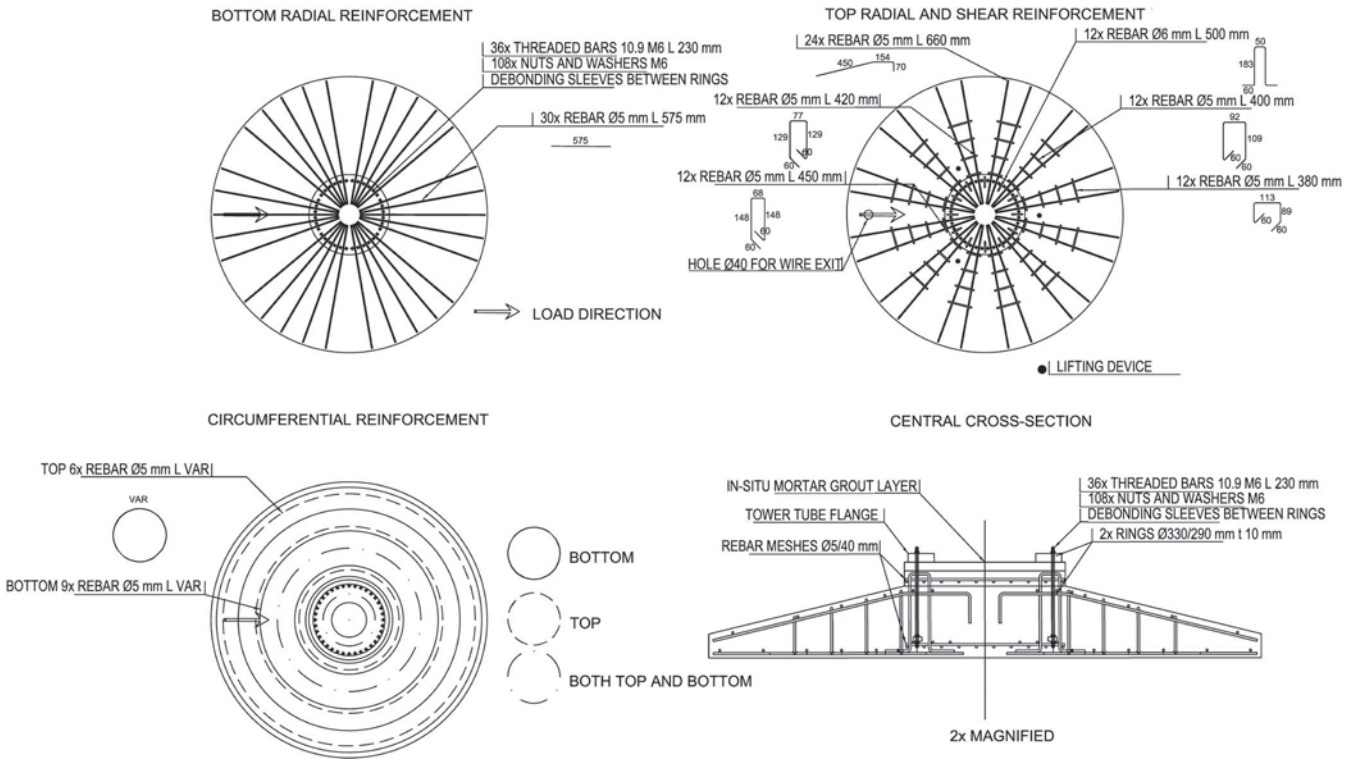

FIGURE 5 Reinforcement details of scaled foundation specimen type FO1

aims of: (i) avoiding mast damage during tests (as the analysis of its response falls beyond the scope of this investigation), (ii) limiting the elastic deformation of the mast, in order to apply a larger rotation to the foundation system given the jack stroke, and (iii) adding a contribution to the increase of vertical loads, necessary, as was previously mentioned, for ensuring stress similarity.

The connection between foundation and tower mast was made by means of threaded bar studs. After the mast temporary installation and the hardening of a high-strength nonshrinking mortar, poured to fill the gap between mast base ring and concrete foundation, the threaded bars were posttensioned along their whole length thanks to the installation of debonding sleeves. For this operation, a mechanical torque wrench was employed, after calibration needed to have similar pre-stress in both model and prototype.

2.2 | Material properties

Concrete class C30/37 was prescribed for all foundation specimens. The mix composition is specified in Table 2 for each specimen. Table 3 collects the results of compressive tests on cubic concrete specimens cast together with the foundations and Brazilian tests on cylindrical core concrete specimens extracted from the tested foundations. The results of these tests highlighted that the actual mean compressive and tensile strengths of concrete resulted higher than those expected from a concrete class C30/37. Table 3 also reports the results of both flexure and compressive tests on prismatic mortar specimens. The results of flexure tests on prismatic notched fiber-reinforced specimens[37] carried out according to EN 14651:2004[40] confirm the relatively large tensile strength of the concrete and show a postcracking behavior corresponding to a class 2B, lower than the expected 3C (*fib* Model Code 2010[41]). This is mainly due to the use, adopted for scaling needs, of small fibers spread into normal concrete. The average R_m and standard deviation σ_{sd} values of residual flexural tensile strength were equal to 3.48 and 0.63 MPa, respectively, for a crack mouth opening displacement of 0.5 mm, and to 2.15 and 0.39 MPa, respectively, for 2.5 mm.

TABLE 2 Concrete mix design (values in kg/m^3)

Components	Mix FO1	Mix FO2	Mix FO3
Cement 52,5 R	260	320	320
Calcareous filler	100	80	80
Sand 0/3 mm	450	450	450
Sand 4/12 mm	1320	1320	1320
Superplasticiser	4.8	7.5	7.5
Water	160	175	175
Fiber OL13/0.16	–	–	70
Total	2295	2353	2423

TABLE 3 Experimental properties of concrete and mortar (d = diameter, L = length, units: mm)

Material	Strength	Test type	Quantity	Age (days)	R_m (MPa)	σ_{sd} (MPa)
Concrete—mix FO1	Compression	Crushing Cube 10 × 10 × 10 cm^3	6	63	58.5	2.00
	Tension	Brasilian on Core Sample d75 L66	1	387	6.05	–
Concrete—mix FO2	Compression	Crushing Cube 10 × 10 × 10 cm^3	16	89	55.5	2.55
	Tension	Brasilian on Core Sample d75 L66	1	191	5.11	–
Concrete—mix FO3	Compression	Crushing Cube 10 × 10 × 10 cm^3	8	108	55.8	2.32
	Tension	Brasilian on Core Sample d75 L66	1	188	8.01	–
Mortar	Compression	Crushing Cube 4 × 4 × 4 cm^3	12	58	74.9	3.52
	Tension	Flexure on Prism 16 × 4 × 4 cm^3	6	58	11.5	1.05

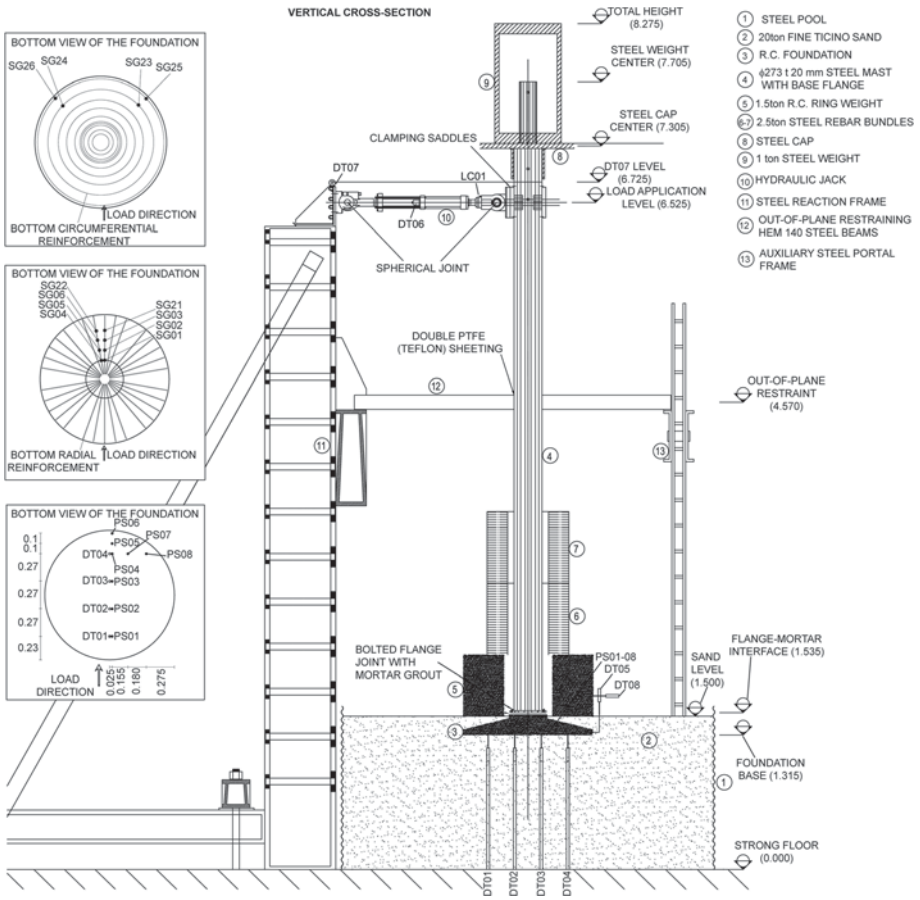

FIGURE 6 Setup cross-section, quotes and external instrumentation. Instrument acronyms are explicated in Table 4 (sizes in [m])

Two groups of steel Ø5 rebars of grade B450A were supplied and employed. The earlier supplied group, employed for the installation of strain gauges and therefore representative of the monitored strains, was characterized by the mean yield stress and ultimate strength values (from standard tensile testing) of 538 and 596 MPa, respectively, whereas the later supplied group, employed for all other noninstrumented reinforcements, was characterized by a mean yield stress and a ultimate strength of 621 and 651 MPa, respectively.

The M6 threaded bars protruding from the foundation, needed to connect the foundation with the S355 steel tower mast, were made of steel class 10.9.

Finally, concerning the foundation soil, standard 300 mm diameter plate compressive tests were carried out in different locations close to the position of the foundation after the soil deposition. From the virgin branch of vertical stress-settlement curves, the estimated secant Young modulus for stress values in between 50 and 100 kPa (the average vertical stress value at the

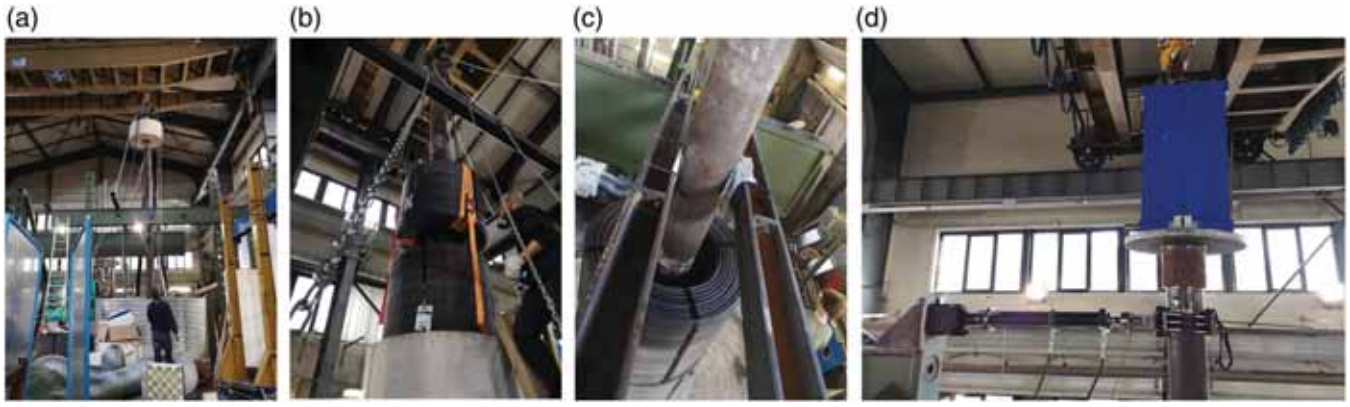

FIGURE 7 Additional elements: (a) positioning of the concrete ring; (b) positioning of rebar coils; (c) restraining beams with double PTFE (Teflon) sheets; and (d) hydraulic jack

TABLE 4 List of instrumentation

Instr. ID	Type	FO1-1	FO1-2	FO2-1	FO2-2	FO3-1	FO3-2	Error (%)	Note
DT01-04	LVDT 40 mm	X	X	X	X	X	X	±0.2	Vertical
DT05	LVDT 40 mm	X	X					±0.2	Vertical
DT06	LVDT 300 mm	X	X	X	X	X	X	±0.01	Horiz. control
DT07	RVDT 750 mm	X	X	X	X	X	X	±0.2	Horizontal
DT08	LVDT 40 mm	X						±0.1	Horizontal
LC01	Load Cell 10 kN	X	X	X	X	X	X	±0.05	Control
SG01-08	Strain Gauge 3 mm	X	X	X	X	X	X	±0.3	On radial bars
SG09-12	Strain Gauge 3 mm	X	X					±0.3	On circ. bars
SG13-20	Strain Gauge 3 mm	X	X					±0.3	On shear bars
SG21-22	Strain Gauge 3 mm			X	X	X	X	±0.3	On radial bars
SG23-26	Strain Gauge 3 mm			X	X	X	X	±0.3	On circ. bars
PS01-08	Pressure Sensor 4.45 kN						X	±3	Below foundation

foundation base corresponding to V_{ULS} in Table 1 is 75 kPa) is equal to 15.3 MPa.

2.3 | Experimental setup

The experimental setup is described in detail in Figure 6. It is composed by the granular soil stratum (#2 of Figure 6), placed in the cylindrical pool (#1 of Figure 6), the foundation (#3 of Figure 6) and the mast (#4 of Figure 6). As previously mentioned, to ensure similarity in terms of vertical stresses both at the levels of the tower-foundation joint and of the foundation-soil interface, additional weights (Figure 7a,b) were positioned on the backfill granular material, above the foundation (one 1.54 t concrete ring and two 2.50 t steel rebar coils, #5–7 of Figure 6) and at the top of the mast (a 1.04 t steel weight over a 0.5 t steel cap, #8–9 of Figure 6).

The horizontal load was imposed by means of a hydraulic jack (#10 of Figure 6 and Figure 7d), installed on a stiff reaction frame (#11 of Figure 6) and regulated by a servocontrolled oil pump. To avoid lateral unintended deviations of the displacement applied by the jack, connected with double spherical hinges to both reaction frame and mast, two restraining beams (#12 of Figure 7c), coated by PTFE sheets to minimize friction, were installed over both reaction frame and auxiliary portal frame (#13 of Figure 6).

The instrumentation, comprising displacement transducers (DT in Figure 6), load cell (LC in Figure 6), strain gauges (SG in Figure 6), and pressure sensors (PS in Figure 6) is described in detail in Table 4.

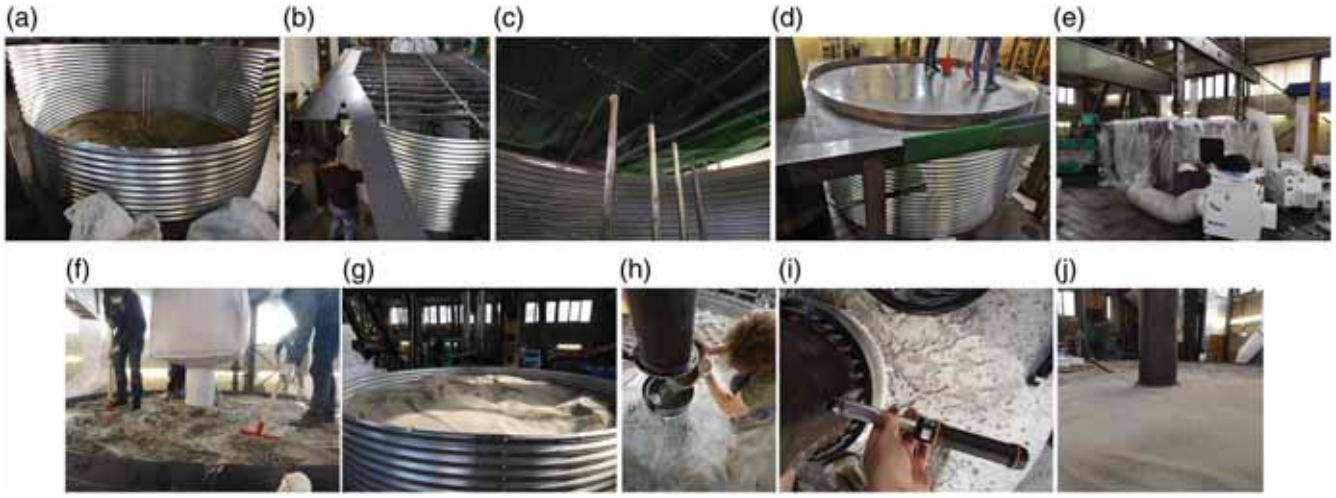

FIGURE 8 Process of assemblage of the setup: (a) cylindric pool assemblage, base waterproofing and installation of the instrument bases; (b) assemblage of the pluviation system; (c) LVDTs installed prior protection and view of the top pluviation system with distribution net; (d) view of the pluviation system from the side; (e) aerial particle protection system with confinement sack and high flow rate fans; (f) sand distribution operations; (g) view of the pool after deposit; (h) pouring of high-strength nonshrinking mortar in mold above foundation; (i) posttensioning of the flanged joint after mortar hardening and mold removal with dynamometric wrench; and (j) view of the tower base after backfill soil distribution

TABLE 5 Test phases

Type	Phase	Description
Vertical	V01	Installation of the concrete ring element
	V02	Installation of the first rebar coil
	V03	Installation of the second rebar coil
	V04	Installation of the top cap with steel mass
Cyclic	C01	Single pseudo-static cycle from 0–0.62 to 0–0.62 H_{ULS} (3.0 kN)
	C02	1000 cycles from 0.41 (2.0 kN) to 0.82 H_{ULS} (4.0 kN); frequency range 0.10–0.22 Hz
	C03	Single pseudo-static cycle 0.62–0.00 to 1.00–0.62 H_{ULS}
	C04	1000 cycles from 0.41 (2.0 kN) to 0.82 H_{ULS} (4.0 kN); frequency range 0.10–0.22 Hz
	C05[a]	200 cycles from 0.06 (0.3 kN) to 0.67 (3.3 kN) H_{ULS}; frequency range 0.10–0.22 Hz
Monotonic	M01	Monotonic pseudo-static load from residual displ. at 0 kN to maximum jack stroke and unload

[a]Only for specimens FO2 and FO3.

2.4 | Preparation of the model

The sand stratum was deposited by using a large pluviation system, consisting in an external steel frame supporting plates with 4 mm diameter holes distributed in regular grids with 50 mm spacing, to ensure repeatability. The sand was deposited from the fixed height of 1850 mm above the strong floor of the laboratory. A suspended plastic grid sheet with 3 mm opening was placed below the pluviation system to increase both sand relative density and deposition homogeneity. The embedded vertical LVDTs were installed before soil deposition. After the pluviation system removal, the sand appeared satisfactorily distributed. After the completion of the series of tests on a foundation specimen, the top 1 m thick sand stratum was removed and redeposited up to the level of the foundation bed after reinstallation of the pluviation system. Subsequently, the

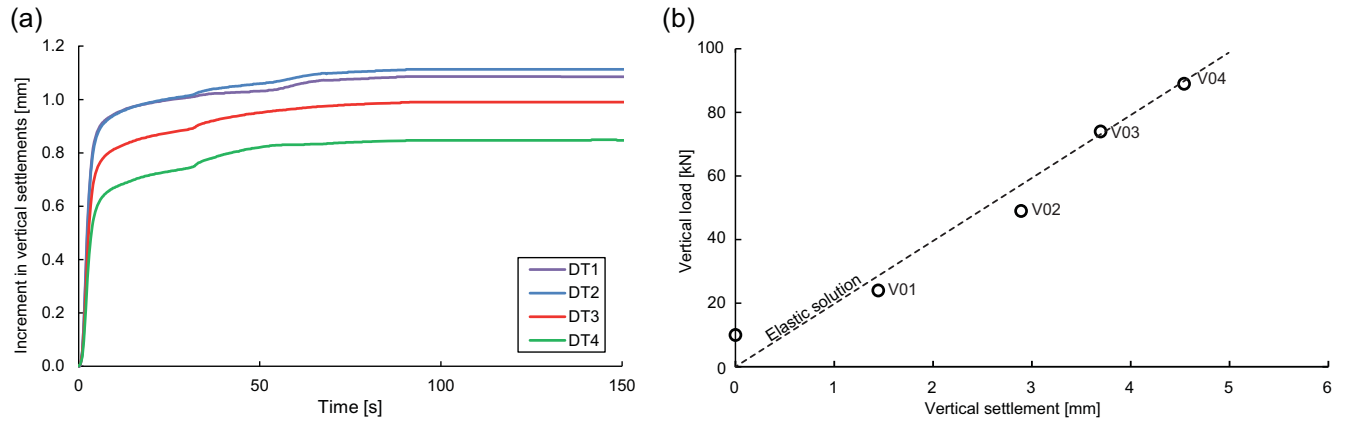

FIGURE 9 Typical results of gravity load tests: (a) settlement tendency under single load application (test V02 of specimen FO2-1), and (b) progressive stiffening under subsequent load applications (tests V01 to V04 of specimen FO2-1)

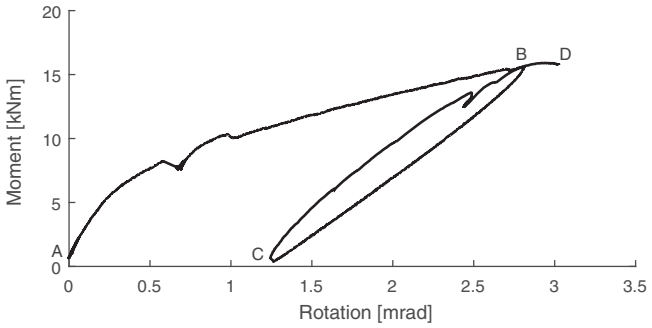

FIGURE 10 Typical results of test C01 with single initial cyclic load application (specimen FO2-1)

foundation was directly positioned over the sand after proper leveling.

The tower mast was then assembled and the high-strength mortar was poured. After mortar hardening, in order to have the same pre-stress of the real prototype, the threaded bars were posttensioned with the help of a dynamometric torque wrench. The backfill soil was later deposited manually.

Pictures of the whole preparation process are collected in Figure 8.

2.5 | Loading phases

As described in detail in Table 5, the tests consist in three subsequent phases:

(1) In this phase, the foundation response under purely vertical loads is investigated. Four vertical load increments (V01-V04), associated with the installation of the additional masses (Figure 7), were applied (Table 5) and the corresponding settlements were measured by means of transducers DT01-04 (Figures 6 and 8).

(2) Five series of cyclic horizontal loads (C01-C05 of Table 5), aimed at investigating the system response under service conditions, were directly applied by the hydraulic jack. The frequency value range was selected according to the limitations of the experimental setup, being it sufficiently low to simulate a quasi-static system response.

The first series (C01) consisted in a single cycle carried out up to a load of 0.62 times the design one. Then 1000 cycles in between 0.41 and 0.82 times the design load were applied (series C02) to investigate the trend of progressive accumulation of permanent rotation. Subsequently, (series C03) a single cycle, carried out up to the design load, was then imposed to compare the mechanical response of first loading with unloading-reloading. This was followed by the further repetition of the previous 1000 cycles (C04) to investigate postpeak-load stability. Finally, 200 cycles with load amplitude varying in between 0.06 and 0.67 times the design load (C05) were carried out to investigate the response under wider cyclic load variation.

(3) A final monotonic push-over under horizontal displacement (M01) was carried out up to maximum stroke of the actuator (equal to 300 mm) aimed at investigating the system behavior close to failure.

3 | EXPERIMENTAL RESULTS

Strains measured on both radial and circumferential reinforcements during both vertical (V01–V04) and cyclic (C01–C05) loading were negligible (i.e., always lower than 2×10^{-5}), implying that the foundation is practically undeformed and uncracked during these stages, and that nonlinear response is limited to the soil. For the sake of brevity, only results obtained from a single test

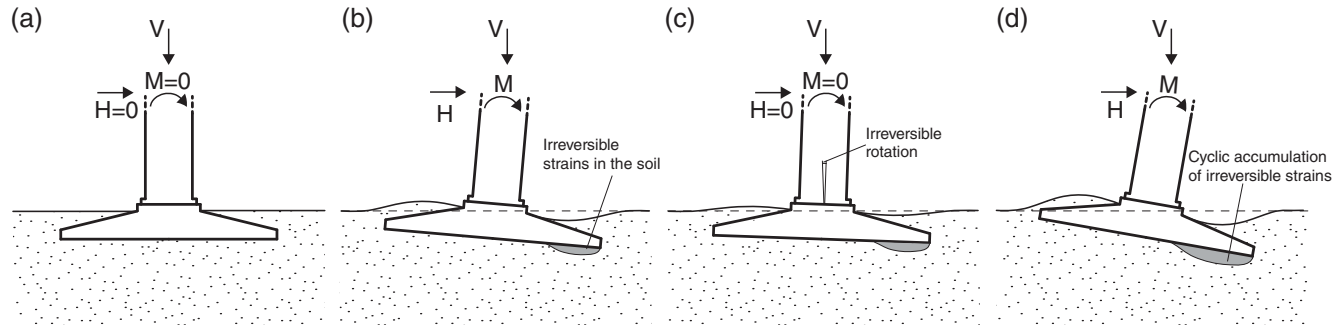

FIGURE 11 Behavior of the tower-foundation-soil system under cyclic loading in service range: (a) initial state, (b) application of lateral load, (c) state after unloading, and (d) behavior under cyclic application of the lateral load

(FO2-1), although also representative of all other, are discussed in the following. In contrast, cracks in the foundation and subsequent strain demand in the instrumented reinforcement were detected from monotonic tests. In this load phase, the system response is dominated by the interaction of foundation and soil nonlinearities.

3.1 | Vertical load tests

As previously anticipated, in this section only the results relative to specimen FO2-1 are discussed. The results of the other specimens are similar, apart from specimen FO1-1. Due to environmental conditions during transportation to the laboratory, prior to the execution of this series of tests the sand was not completely dry during deposition and, thus, relative density was found out to be slightly lower with respect to the further tests.

The total vertical settlement (ζ) under a single vertical load (V) application (Figure 9a, corresponding to phase V02) can be decomposed as the sum of (i) an almost instantaneous contribution at load application, and (ii) a delayed contribution due to time needed for the rearrangement of the sand grain sub-structure.[42] To be noted that the latter contribution tends to be asymptotic and stabilizes after a time range limited to only about 2 min.

The maximum settlements measured in test phases V01–V04 (circles) are plotted in Figure 9b. The initial (nonnull) value of V corresponds to the self-weight of foundation, steel tower and the backfill soil. The experimental points relative to phases V01–V04, tend to be aligned with the slope associated with the classical solution for rigid circular shallow foundations on an elastic halfspace[43] (dashed line of Figure 9b):

$$V = \frac{DE}{1-\nu^2}\zeta, \tag{1}$$

where the Poisson ratio ν is set to 0.25, while E is imposed to be equal to the secant soil stiffness value (50–100 kPa range) estimated from the results of the previously cited plate tests. Small deviations from linearity suggest a slightly stiffening trend with the load.

The quasi-linear load-settlement curve indicates that the final load value is significantly smaller with respect to the bearing capacity under vertical centered loads. In this case, the ULS vertical load value (V_{ULS} of Table 1) is approximately equal to 1% of the bearing capacity under vertical loads, estimated by means of the expression proposed by Meyerhof.[44]

3.2 | Cyclic load tests

The results relative to test C01 (Table 5) are plotted in Figure 10 in the M-θ plane, being M the applied moment, and θ the base rotation calculated as follows:

$$\theta = (\delta - \delta_{el})/l_b = \left(\delta - \frac{3EI}{h^3}\cdot H\right)/l_b \tag{2}$$

being δ the top displacement measured by DT07 (Figure 6), δ_{el} the elastic deformation of the steel mast, l_b the distance of DT07 to the base of the foundation, h the height of the mast up to loading point and EI the elastic bending stiffness of the steel tube. In this case, second-order effects are negligible, and therefore, M is calculated as the horizontal load (H) multiplied by the lever arm between the base of the foundation and the jack axis (l).

The results highlight that the system response is nonlinear from the early stages of the loading process. The initial loading branch (A-B) is significantly softer than the unloading (B-C) and the reloading (C-D) branches, suggesting the accumulation of irreversible strains in the soil. The unloading-reloading branch is associated with a hysteresis loop. The inversion in sign in the

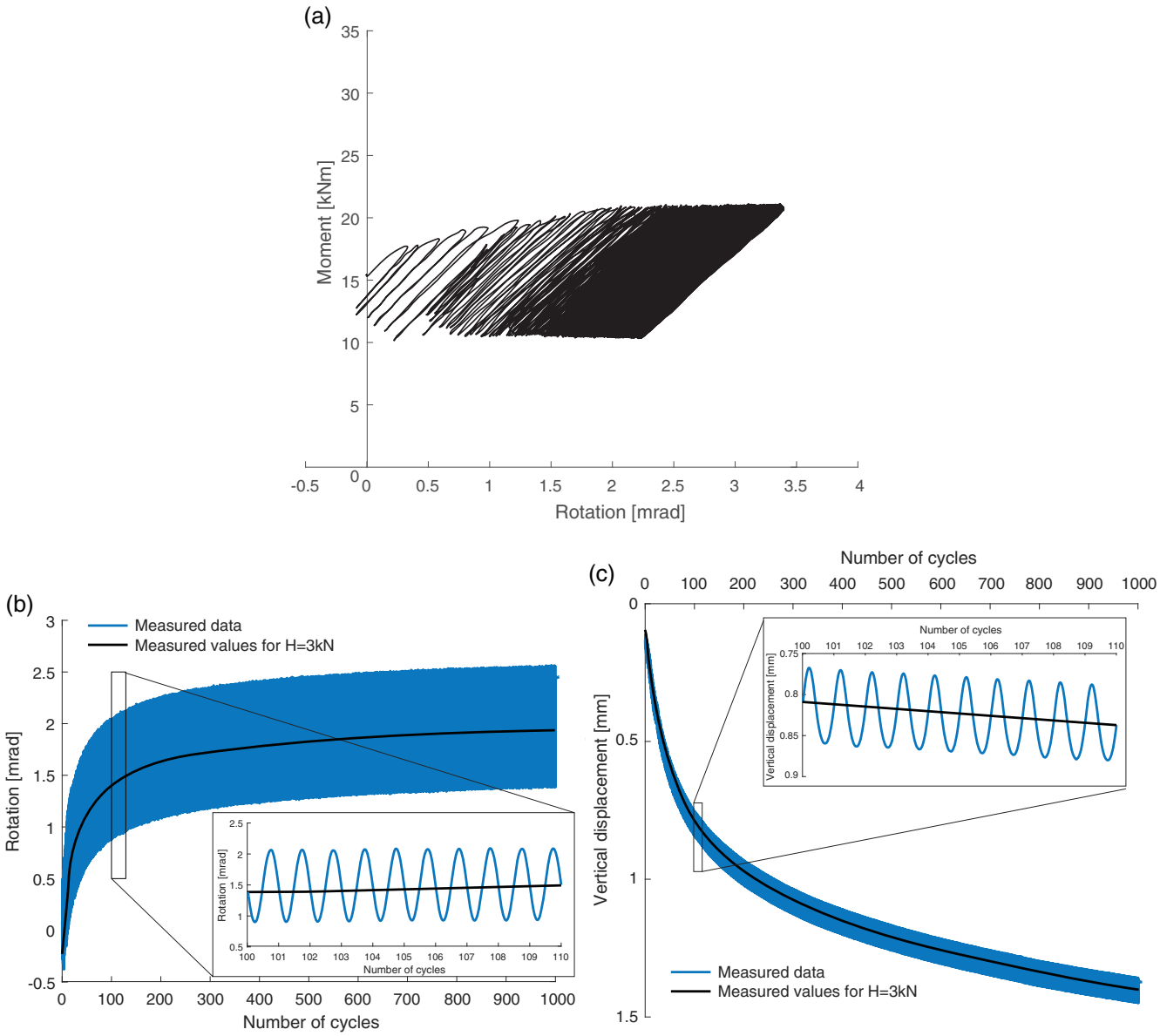

FIGURE 12 Typical results of test C02 with 1000 load cycle repetition (specimen FO2-1): (a) hysteresis, (b) trend of accumulation of irreversible rotation through cycles, and (c) trend of accumulation of mean vertical settlement through cycles

rotation increments is delayed with respect to the inversion in sign in moment increments. Analogously to what previously commented, this is due to the time necessary for sand sub-structure rearrangement to occur.[45]

For the sake of clarity, a schematic representation of the system response in the first loading-unloading-reloading cycle is sketched in Figure 11 (Figure 11a-d represent the system configuration at points A, B, C, D of Figure 10, respectively).

The results of cyclic tests C02 (Table 5) denote a progressive accumulation of both irreversible rotations and vertical settlements (Figure 12). This ratcheting process is characterized by a stabilization of the system response, that is, a progressive reduction in the accumulation rate.

During tests C03 (Figure 13a), the response is practically linear up to the maximum load value imposed in the previous tests (ABC Figure 13a). For larger H values, the response becomes nonlinear and irreversible rotations develop (CD Figure 13a). Even if the maximum M value coincides with the ULS one (Table 1), strains in the reinforcements (both radial and circumferential) were negligible for all the foundations tested, implying that nonlinearities are only due to the soil mechanical behavior.

The subsequent loading phases C04 (Figure 13b) and C05 (Figure 13c) are characterized by a different amplitude (1.0 and 1.5 kN, respectively) and mean (3.0 and 1.8 kN, respectively) values. In both cases, accumulation in

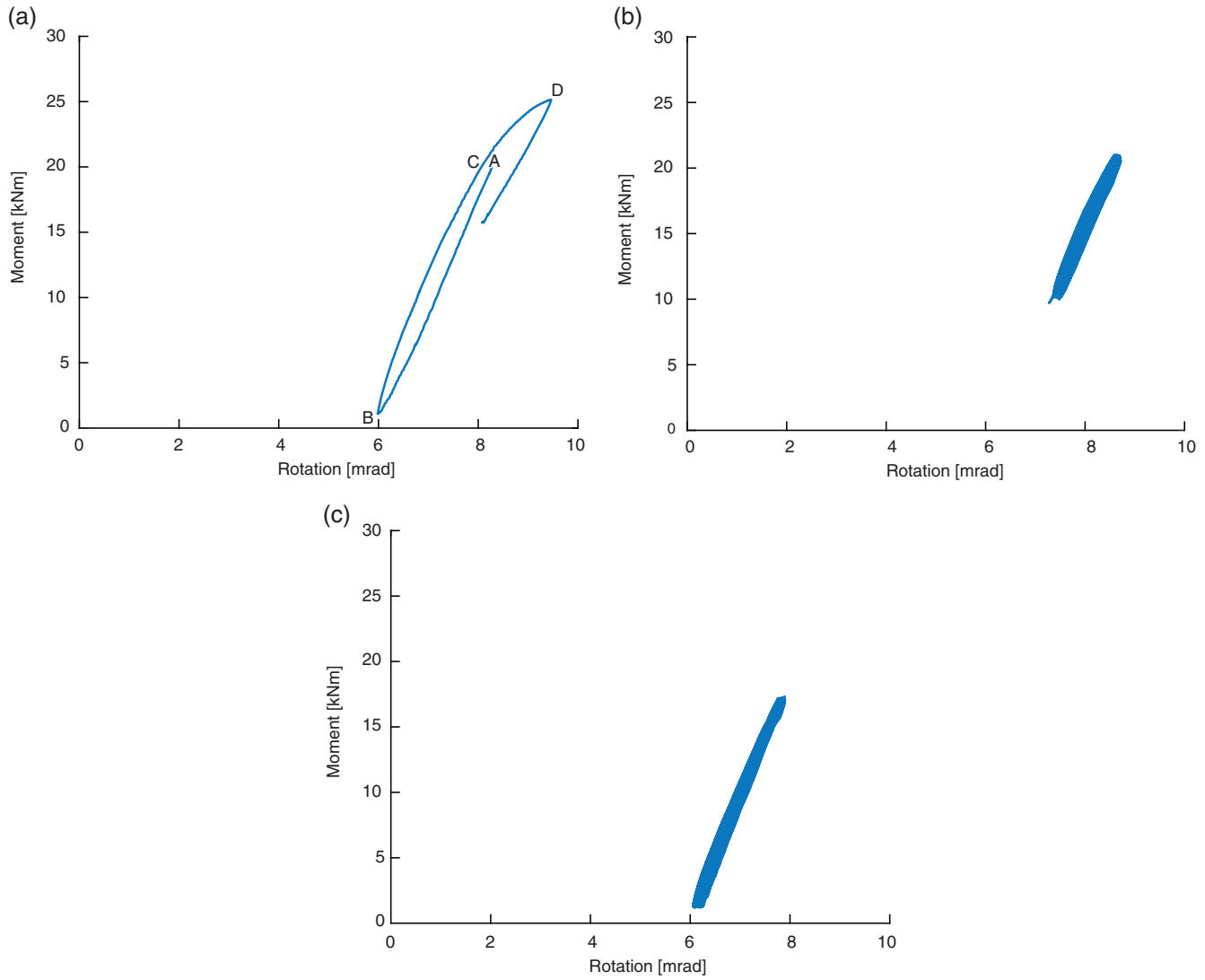

FIGURE 13 Typical results of tests (a) C03 (specimen FO2-1), (b) C04 (specimen FO2-1), and (c) C05 (specimen FO2-1)

rotations is practically negligible, implying that the system reached a plastic adaptation regime.

3.3 | Monotonic displacement tests up to setup limit

All the displacement-controlled monotonic tests (M01 of Table 5) were conducted until the attainment of the maximum stroke of the jack, equal to 300 mm (6% of drift ratio). The initial state of the structural assembly and its deformed state in correspondence of the maximum drift are compared in Figure 14. It is worth noting that the crane is connected to the top of the assembly for safety reason only, the sling being loose during the entire test execution.

In this case, for the calculation of M, second-order effects associated with the masses positioned at the top of the mast could not be considered negligible. They were introduced according to the following equation:

$$M = H \cdot l + \frac{\delta}{l_b} \cdot (\mathrm{V}^* \cdot \mathrm{d}^* + \mathrm{V}^{**} \cdot \mathrm{d}^{**}), \tag{3}$$

being V^* the weight of the top steel mass and V^{**} the weight of the top steel cap, respectively, whereas d^* and d^{**} the distance of their center of mass from the bottom of the foundation.

For the sake of clarity, the results relative to one single test (FO2-1) are discussed firstly. In particular, the results are plotted in the M-θ plane in Figure 15a, whereas radial and circumferential strain gauge measurements are plotted versus the base rotation θ in Figure 15b,c, respectively. Finally, in Figure 15d strain gauges position is shown, together with the observed crack pattern at the end of the test.

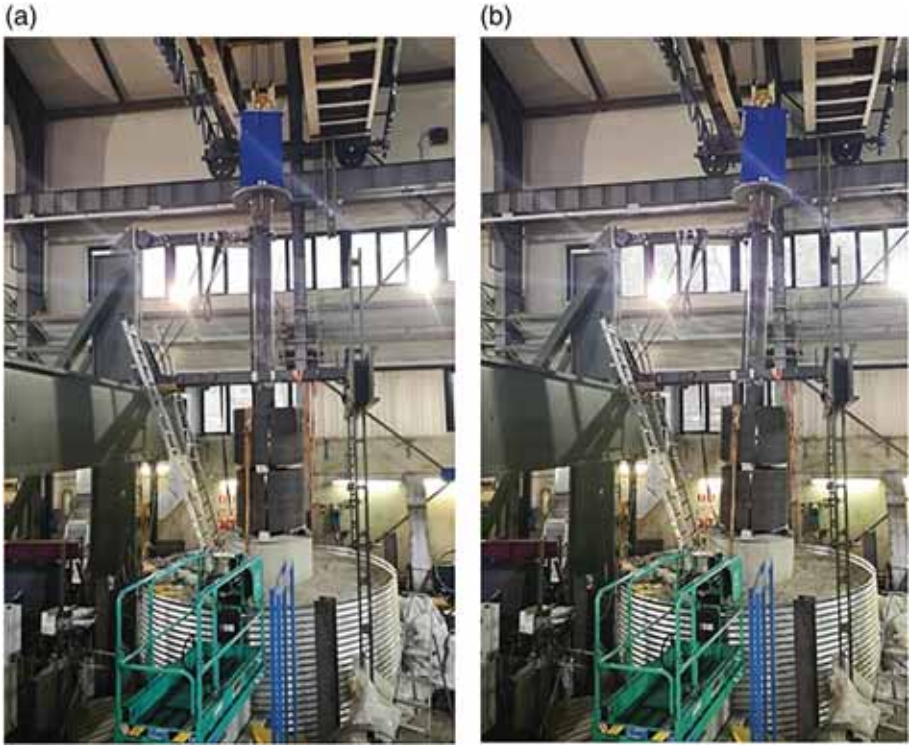

FIGURE 14 Picture of full assembly during monotonic test M01 (specimen FO3-2) at (a) beginning and (b) maximum drift

The initial θ value is not null, due to the accumulation of irreversible displacement in the foundation soil during the cyclic tests. The results in the M-θ plane seem to be practically linear up to the maximum load applied in the previous cyclic loads (O-A in Figure 15a, up to $H = 4.9$ kN and $M = 24.1$ kNm). For these load values, circumferential strains are very small, while radial ones are practically null. After this first stage, the response in the M-θ plane becomes remarkably nonlinear (A-B), radial strain gauges measurements progressively increase, while circumferential ones are still negligible.

At point B, for increasing θ values, a sudden reduction in M value is observed. This temporary softening is associated with a very sharp increase in strains of SG2 (Figure 15b), SG23,25,26 (Figure 15c) and with a moderate increase in strains of both SG1 and SG2 (Figure 15b). All these measurements suggest the opening of crack 1 of Figure 15d (developing in between SG1,4 and SG2,5), later visually detected, after the extraction of the foundation specimen from the soil. From point B to C, due to the static redundancy of the system, an increment in M is observed. At point C, a second softening occurs (Figure 15a). This second jump is likely to be associated with the formation of the second crack (Figure 15d), as also detected by the sharp increase in measurements of SG3 and SG6 (Figure 15b). Even in this case, the system is not at failure, as the global response hardens until point D, where the maximum value of M is obtained. From C to D, strains in SG3 and SG6 become remarkably large (higher than 0.2%), suggesting the radial rebar yielding. Moreover, remarkable strains are measured even by SG21 and SG22 (Figure 15b), almost not activated for lower M values. A faint softening mostly attributable to second-order effects is observed until point E, corresponding to the jack maximum stroke.

Finally, the unloading stage (E-F) is characterized by a progressive increase in stiffness. The final stiffness of the system is noticeably lower than the initial one and very large values of irreversible rotations (Figure 15a) and residual strains (Figure 15b,c) are evident at point F (Figure 15a).

For the sake of completeness, displacements of DT01 and DT04, recorded during the monotonic test, are plotted in Figure 16 (points A-F corresponds to points A-F of Figure 15a). The curve corresponding to DT01 is always characterized by negative (upward) displacements. The final point of this curve is associated with detachment of the foundation from the LVDT, implying that the foundation detaches from the soil, too. The readings by DT04 clearly show the accumulation of irreversible (downward) displacements.

Further insights concerning the above-described mechanisms are provided by the readings of the pressure sensors. To be noted that the pressure values over soil measured by pressure sensors are influenced by the similarity between reading surface of the sensor and sand grain dimensions and, hence, the absolute values of the obtained readings are to be only qualitatively considered.

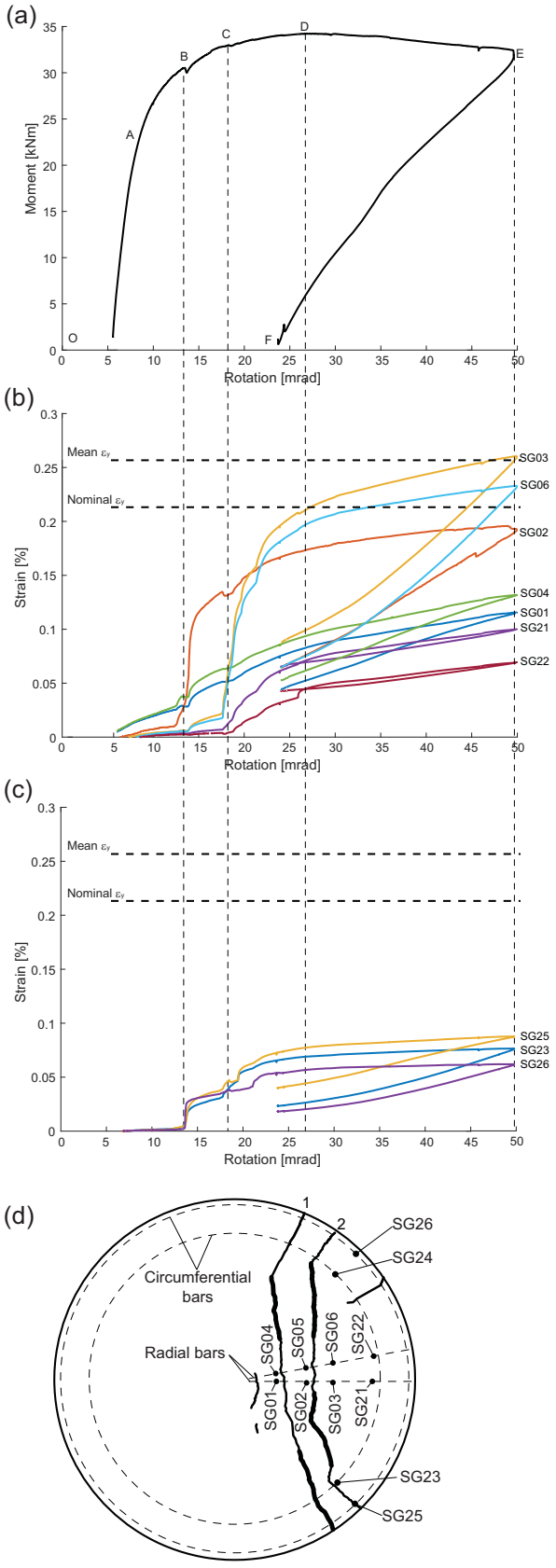

FIGURE 15 Typical results of monotonic test M01 (specimen FO2-1): (a) moment versus rotation monotonic curve, (b) strain of radial rebars, (c) strain of circumferential rebars, and (d) crack pattern and position of strain gauges

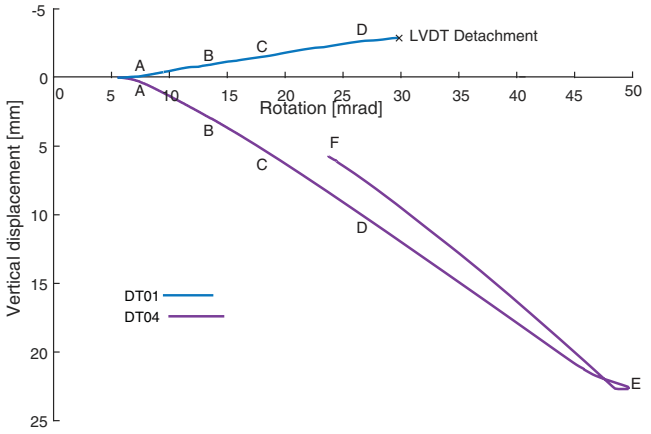

FIGURE 16 Evolution of vertical displacements at the foundation base during monotonic loading (specimen FO3-2)

Nevertheless, their trend is explicative. Referring to the alignment parallel to the load direction (Figure 17a), as soon as after 2 mrad of mean rotation, the foundation lifted off the two pressure sensors closer to the jack position (PS01 and PS02), with the third (PS03) located over the foundation center of gravity also lifting off after around 15 mrad, in the range of the formation of the first flexural crack. At the same time, the front pressure sensors (PS04 and PS05) detected an increase in vertical stress, with PS04 detecting a maximum stress value at about 25 mrad of rotation, followed by a softening branch associated with the further displacement of the resultant towards the edge, as indicated by the contemporary increase of the reading of the outer sensor PS05. The edge instrument (PS06), too close to the foundation boundary, did not detect any relevant amount of stress. In the unload phase, due to the accumulation of irreversible rotations, PS04 measured again the maximum stress, but associated to the much higher rotation of 40 mrad, after which it decreased due to the further recentering of the resultant towards the center, as noticed by the increment of stress in the inner instrument (PS03), which came back into contact with the foundation soon after the displacement inversion. Referring to the transverse alignment located at 400 mm from the center (Figure 17b—PS04, PS07, and PS08), the different pressure trends indicate a progressive loss of stiffness of the foundation element, mainly caused by cracking.

The behavior of the soil-foundation system is summarized by the sketches reported in Figure 18: (i) as previously mentioned, at the beginning of the test phase, residual deformations are present (Figure 18a), (ii) the increase in both M and H induces the accumulation of additional irreversible strains in the foundation soil (Figure 18b, corresponding to branch A-B of Figure 15a), (iii) for sufficiently large M and H values, cracks

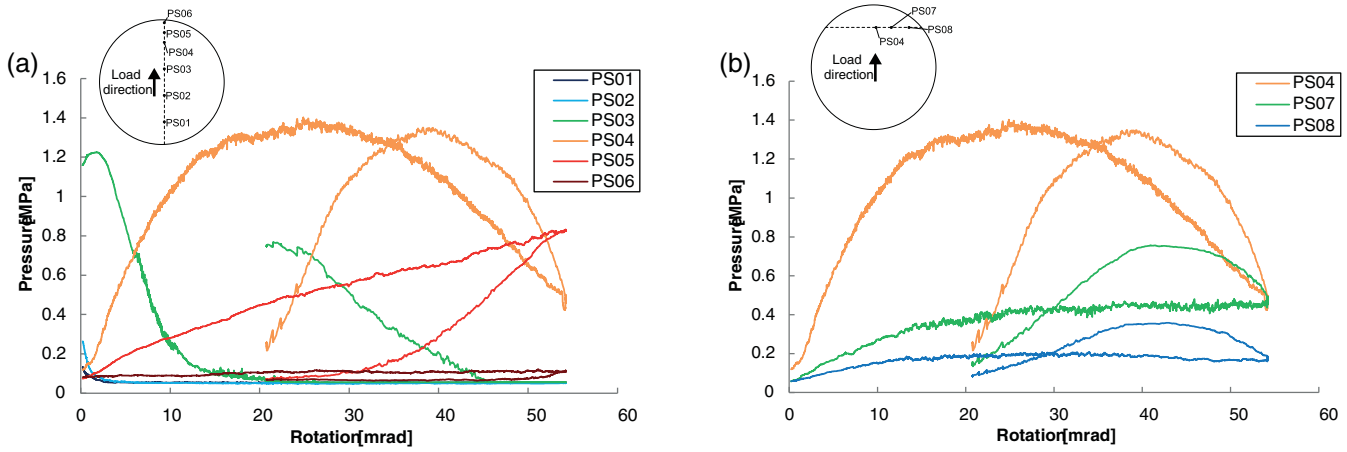

FIGURE 17 Readings from pressure sensors through monotonic test (specimen FO3-2): (a) longitudinal alignment and (b) transverse alignment

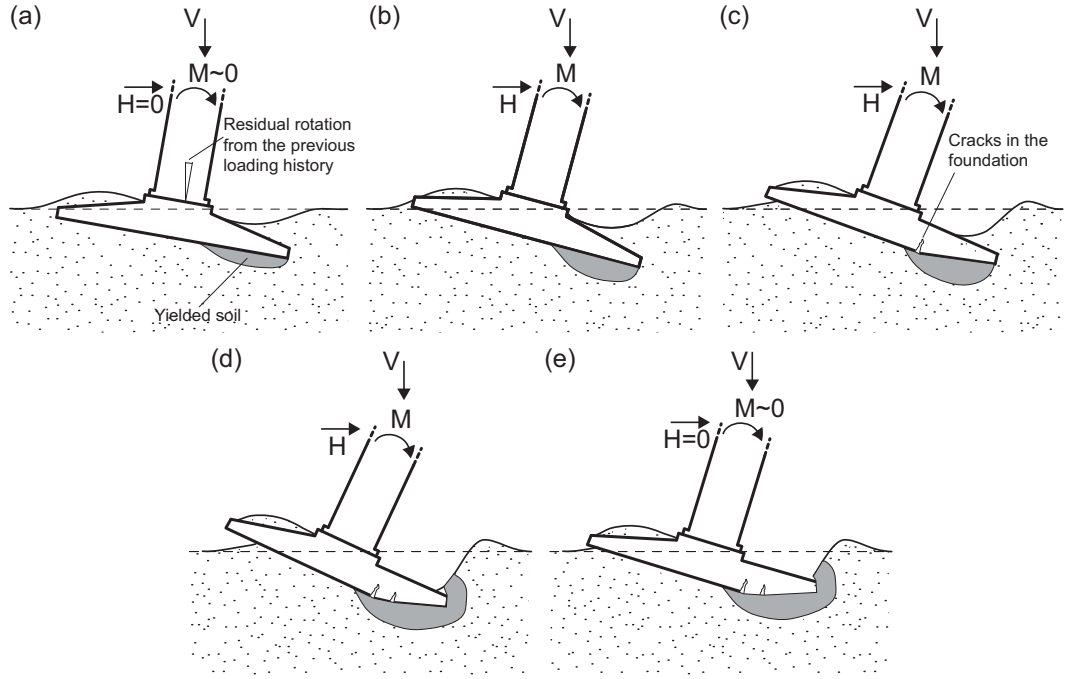

FIGURE 18 Behavior of the tower-foundation-soil system under ultimate loading: (a) initial state with residual deformation from previous tests, (b) application of lateral load, (c) crack opening in the foundation and progressive localization of stress in the soil, (d) system failure, and (e) unloading and crack closure

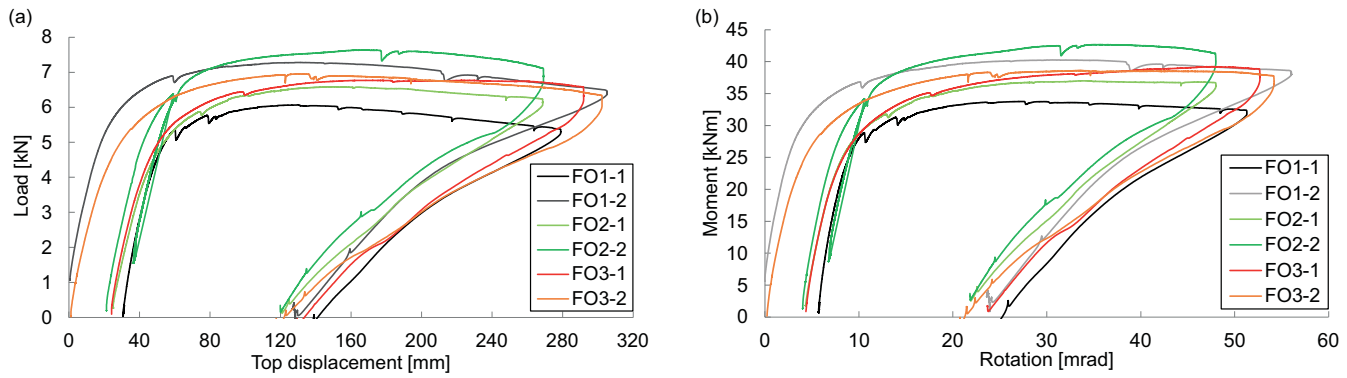

FIGURE 19 Results of monotonic tests: (a) shear load versus top displacement and (b) overturning moment versus base rotation

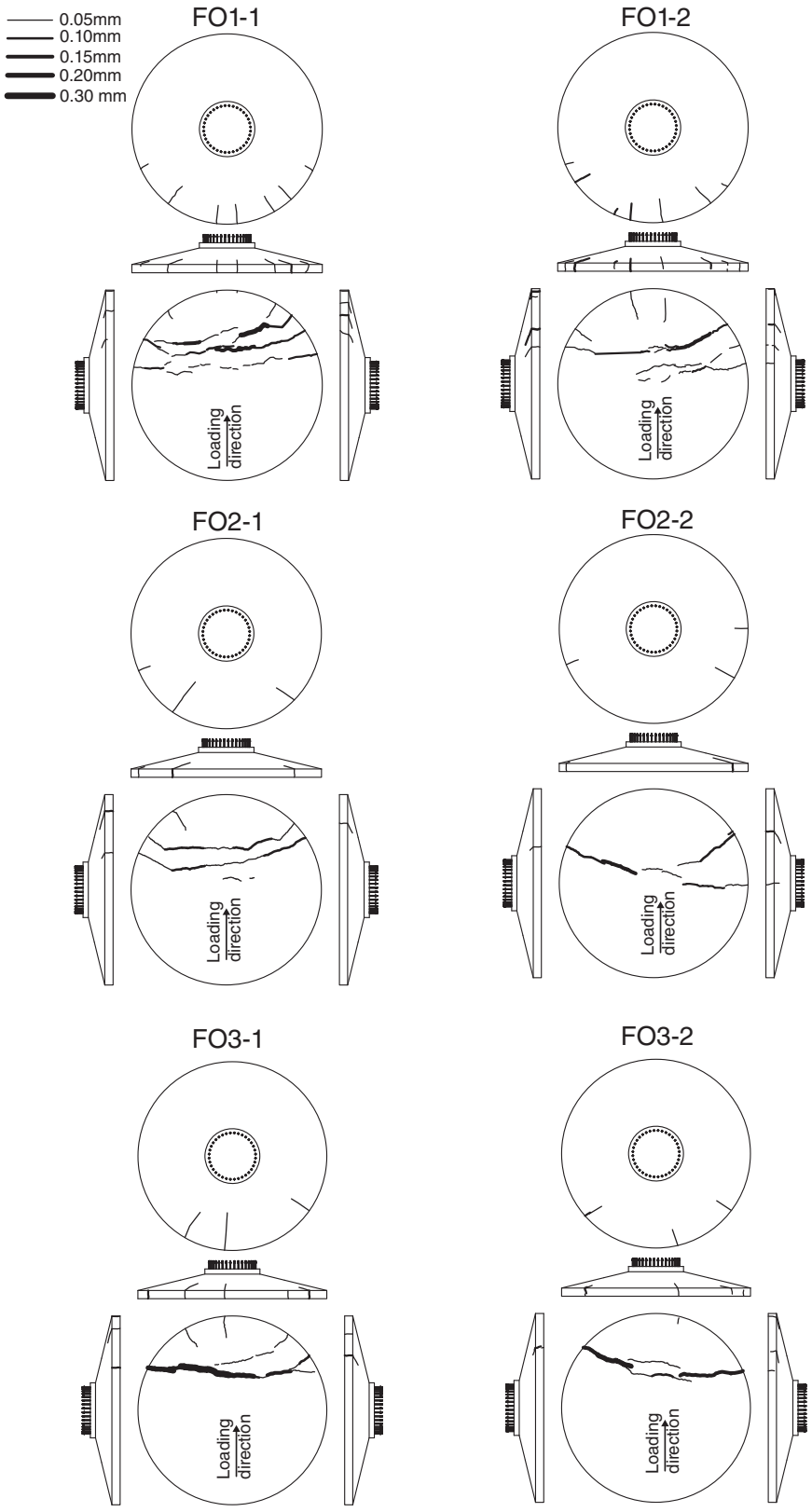

FIGURE 20 Crack patterns

development, reinforcements yielding and consequent formation of plastic hinges (B-D of Figure 15a) imply a severe reduction in the foundation-soil contact area, and therefore, the progressive localization of both stresses and strains in the soil close to the foundation edge (Figure 18c), (iv) finally ultimate conditions are reached

(Figure 18d) and (v) the progressive stiffening during the unloading is associated with both cracks closure and with the increase in contact area. The difference in the slope of initial loading (O-A of Figure 15a, almost elastic) and final unloading branches of the M-θ curve is due on one side to the damage of the foundation and, on the other side, on the accumulation, even during unloading, of irreversible strains in the soil[46] causing an evolution of the foundation geometrical configuration (second-order effects).

The results of all monotonic tests M01 are plotted in Figure 19 in terms of H-δ and M-θ. All the curves present very similar initial (during loading) and final (during unloading) slopes. For all the cases considered, both ultimate horizontal force (ranging from 6.0 to 7.6 kN) and moment values (ranging from 32 to 40 kNm) are larger than the corresponding (scaled) ULS load ones (4.9 kN and 24.1 kNm, Table 1). The lowest ultimate load value is obtained for test FO1-1, the first performed. In that case, as was previously mentioned, the deposited soil had a certain degree of moisture due to environmental conditions during transportation to the laboratory. For this reason, the soil relative density (and therefore, bearing capacity) was slightly lower for the first specimen with respect to the next ones. Even if foundation specimens are identical couples, a slight dispersion in the results can be observed, but the difference with respect to the average value is always lower than 10%, which may predominantly be attributed to the imperfections of the manual leveling of the sand prior to the installation of the foundation. Despite the reinforcement arrangements in the foundation specimens are significantly different, the ultimate values of H and M are similar, implying that, from a practical point of view, the three reinforcement systems can be considered equivalent.

In all monotonic curves (Figure 19) sudden local downward spikes, associated with progressive formation of cracks, are evident.

The crack patterns at the end of the test reported in Figure 20, highlight a combination of horizontal cracks developed in the lower foundation face running almost orthogonal to the load direction, and radial slicing cracks propagated on the edge of the foundation opposite to the point of load application (Figure 21). The former ones are due to bending, and the latter ones are due to radial inclined struts developed in the foundation. The compressive force (C) transferred by the struts is equilibrated by tensile forces (T) in circumferential rebars (Figure 21). It is worth noting that flexural cracks at the top of the foundation were never detected.

The crack patterns for foundations FO1 and FO2 (with and without stirrups) are similar, without revealing shear cracks or shear-related failure modes. This is also confirmed by the practically null values of strains measured by strain gauges installed on stirrups in specimens FO1. In these cases, two main flexural cracks developed. By interpreting the strain gauge measurements as per Figure 15, in all cases the first flexural crack opened in the proximity of the foundation center, with further flexural cracks eventually opening towards its edge.

In case of FO3, despite the presence of the fibers, a single well-defined crack developed. In both FO3-1 and

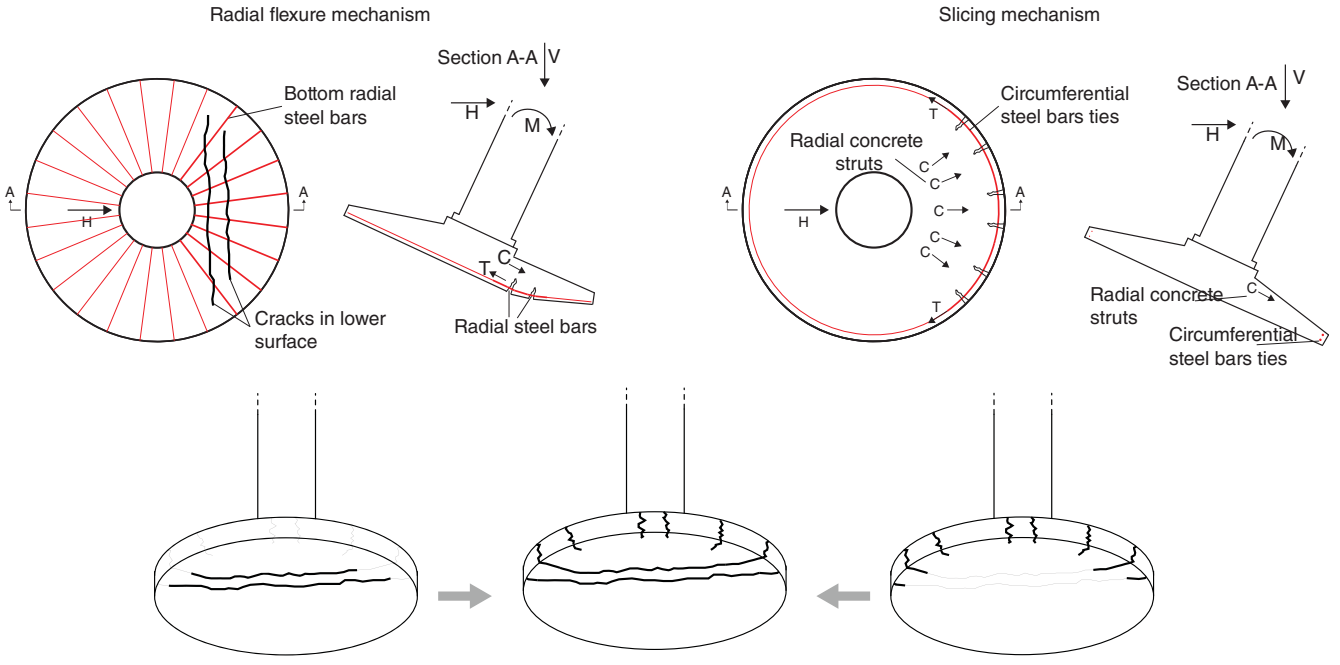

FIGURE 21 Interpretation of the crack pattern observed

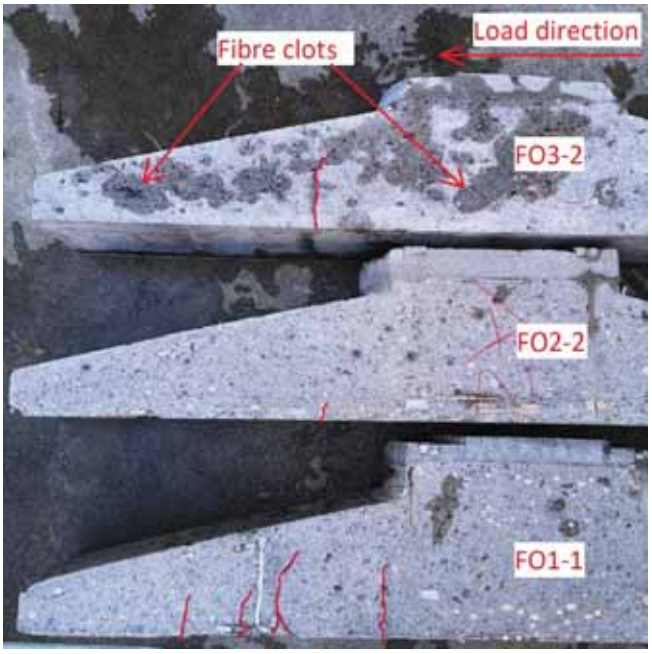

FIGURE 22 Cut specimens in 16 cm wide central slices with crack penetration marked in red

FO3-2 the crack width was significantly larger with respect of those of FO1 and FO2, implying the addition of fibers was less effective than the half of radial and circumferential reinforcement removed, at least in terms of crack diffusion.

This can be justified by (i) the relatively low strength of the concrete matrix associated with the very short fibers employed and (ii) the heterogeneous distribution of fibers. In fact, as shown in Figure 22, containing pictures of the slices of one of each foundation typology after cutting of a central 160 mm wide slice parallel to the load direction, several fiber clots were present in the foundation, due to the large quantity and very small dimension of fibers.

In Figure 22 the typical diffusion of the cracks along the depth of the foundation element, with vertical flexural cracks inclining towards the foundation center at the top due to the interaction with shear, is shown. For all foundation specimens, cracking did not develop inside the central foundation cylinder in correspondence of the foundation-tower joint.

4 | CONCLUSIONS

The experimental evidence under service load range highlights that, for the cases investigated, the reinforced concrete foundation elements are not subject to damage or any irreversible process. On the contrary, cyclic wind-induced lateral loads cause the accumulation of irreversible strains in the foundation soil, associated with a progressive accumulation in irreversible rotations and, even if vertical loads are kept constant, irreversible vertical settlements. These accumulations, however, are asymptotic, that is, rotation and settlements are accumulated at a progressively decreasing rate, implying that the system reaches a plastic adaptation regime.

Under ultimate load conditions, all the reinforcement solutions analyzed are characterized by similar behavior and strength, remarkably higher than the design load, and they are therefore to be considered practically equivalent from a structural performance point of view. The observed failure mode for all the foundation specimens is characterized by the contemporary development of cracks in the foundation element with moderate yielding of the radial reinforcement, and attainment of the soil bearing capacity in a highly localized area relatively close to the border of the foundation. This combined failure highlights how soil-structure interaction affects the foundation bearing capacity.

The crack patterns observed were similar through all the tests, with the formation of main horizontal flexural cracks orthogonal to the load direction at the bottom of the foundation and slicing vertical cracks due to the formation of inclined compressive struts. The softening behavior shown by bending tests of fiber-reinforced concrete specimens carried out to characterize the material negatively affected the behavior of the third reinforcement system, characterized by the half of radial and circumferential reinforcement, preventing the propagation of diffuse cracks in the foundation. This was due to the combination of a relatively weak concrete matrix and small fibers employed for scaling reason, not allowing for the full development of the expected postcracking behavior, which is however seen in favor of safety for the tested specimens. Nevertheless, the adoption of metallic fibers in partial replacement of traditional steel rebars for wind tower foundations appears a smart and promising option to be pursued.

The outcomes of the experimental activity suggest that a relevant optimization of the foundation reinforcements, associated with time, labor and material savings, can be promisingly achieved. It is worth mentioning that the absence, necessary for scaling reason, of large aggregates in the concrete mix led to relatively large concrete tensile and shear strength, which may have limited the development of the crack pattern. To investigate this aspect, the authors carried out a series of numerical analyses aimed at reproducing the experimental results[47] and they are currently investigating the response of full-scale prototypes, by checking the eventual development of alternative failure modes related to either shear or local stress concentrations in the central area of the foundation.

ACKNOWLEDGMENTS

The experimental activity is part of a wider research grant agreement stipulated among the Departments of Civil and Environmental Engineering, Mechanics, Energy, and Management Engineering of Politecnico di Milano and Enel Green Power Spa. Magnetti Spa is acknowledged for the production of the concrete specimens. Acknowledgements are also due to Daniele Spinelli, Giacomo Vazzana, Marco Antico, and Gabriele Frigerio for their help in carrying out the tests.

DATA AVAILABILITY STATEMENT

The data that support the findings of this study are available from the corresponding author upon request.

ORCID

Bruno Dal Lago https://orcid.org/0000-0002-3088-8376
Luca Flessati https://orcid.org/0000-0002-9586-3057
Paolo Martinelli https://orcid.org/0000-0003-1029-7744
Claudio di Prisco https://orcid.org/0000-0002-9245-6587
Marco di Prisco https://orcid.org/0000-0003-1779-2449

REFERENCES

1. Hansen MOL, Sørensen JN, Voutsinas S, Sørensen N, Madsen HA. State of the art in wind turbine aerodynamics and aeroelasticity. Prog Aerospace Sci. 2006;42:285–330.
2. McKenna R, Ostman v.d. Leye P, Fichtner W. Key challenges and prospects for large wind turbines. Renew Sustain Energy Rev. 2016;53:1212–21.
3. DNV/Risø. Guidelines for Design of Wind Turbines. Copenhagen, Denmark: Det Norske Veritas (DNV) & Risø National Laboratory; 2002.
4. Gasch R, Twele J. Wind power plants: fundamentals, design, construction and operation. 2nd ed. Berlin, Germany: Springer; 2012.
5. Andersen LV, Clausen J. Efficient modelling of wind turbine foundations. In: Carriveau R, editor. Fundamental and advanced topics in wind power. London, UK: IntechOpen; 2011. p. 115–74.
6. Ma Y, Martinez-Vazquez P, Baniotopoulos C. Wind turbine tower collapse cases: a historical overview. Proc. Inst. Civ. Eng.: Struct. Build. 2018;172:547–55.
7. Chou JS, Tu WT. Failure analysis and risk management of a collapsed large wind turbine tower. Eng Fail Anal. 2011;18:295–313.
8. Bonnett D. Wind turbine foundations: loading, dynamics and design. Struct Eng. 2005;3:41–5.
9. Mohamed W, Austrell PE. A comparative study of three onshore wind turbine foundation solutions. Comput Geotech. 2018;94:46–57.
10. Lavassas I, Nikolaidis G, Zervas P, Efthimiou E, Doudoumis IN, Baniotopoulos CC. Analysis and design of the prototype of a steel 1-MW wind turbine tower. Eng Struct. 2003;25:1097–106.
11. Matos RP, Pinto PL, Rebelo CS, Gervasio HS, Veljkovic M. Improved design of tubular wind tower foundations using steel micropiles. Struct Infrastruct Eng. 2016;12(9): 1038–50.
12. Lombardi D, Bhattacharya S, Muir Wood D. Dynamic soil-structure interaction of monopile supported wind turbines in cohesive soil. Soil Dyn Earthq Eng. 2013;49:165–80.
13. Hassanzadeh M. Cracks in onshore wind power foundations: causes and consequences. Elforsk Rapp. 2012;11:56.
14. Fujiyama C, Koda Y, Sento N. Evaluation and stability analysis of onshore wind turbine supporting structures. In: Okedu KE, editor. Stability control and reliable performance of wind turbines. London, UK: IntechOpen; 2018; p. 103–19.
15. Bai, X., Ma, R., He, M. & Huang, D. 2016: Structural condition monitoring of wind turbine foundations. Proceedings of the Institution of Civil Engineers, 2016, 1600012.
16. Bai X, He M, Ma R, Huang D, Chen J. Modelling fatigue degradation of the compressive zone of concrete in onshore wind turbine foundations. Construct Build Mater. 2017;132:425–37.
17. Berardengo M, Manzoni S, Vanali M, Lucà F. One year monitoring of a wind turbine foundations. Spec Top Struct Dyn Exp Tech. Cham, Switzerland: Springer International Publishing; 2020;5.
18. Currie, M., Saafi, M., Tachtatzis, C. and Quail, F., 2013: Structural and health monitoring for wind turbine foundations. Proceedings of the Institution of Civil Engineers, 1200008, 166, 162, 169.
19. McAlroum J, Perry M, Fusiek G, Niewczas P, McKeeman I, Rubert T. Deterioration of cracks in onshore wind turbine foundations. Eng Struct. 2018;167:121–31.
20. Ripa-Alonso T, González-Dueñas E. Cracks analysis in onshore wind turbine foundations. Proceedings of the 37th IABSE symposium. Volume 112. Zurich, Switzerland; International Association for Bridge and Structural Engineering; 2014; p. 1086–92.
21. Perry M, McAlorum J, Fusiek G, Niewczas P, McKeeman I, Rubert T. Crack monitoring of operational wind turbine foundations. Sensors. 1925;2017:17.
22. Fujiyama C, Yonetsu K, Maeshima T, Koda Y. Identifiable stress state of wind turbine tower-foundation system based on field measurement and FE analysis. Proc Eng. 2014;95:279–89.
23. Gondle RK, Kurup PU, Niezrecki C. Evaluation of wind turbine-foundation degradation. Proceedings of the international conference of the international association for computer methods and advances in geomechanics: challenges and innovations in geomechanics. Innsbruck, Austria: International Association for Computer Methods and Advances in Geomechanics; 2021. p. 21–8.
24. Fuchs W, Meyer J, Hartwig T. Strengthening and retrofitting of onshore wind turbine foundations. Bauingenieur. 2013;88: 307–16.
25. He M, Bai X, Ma R, Huang D, Liu H. Field experimental study on the retrofit of cracked onshore wind turbine foundations using externally prestressed anchor bolts. Struct Concr. 2018; 19:864–75.
26. Adhikari S, Bhattacharya S. Vibrations of wind-turbines considering soil–structure interaction. Wind Struct. 2011;14: 85–112.
27. Bernuzzi C, Crespi P, Montuori R, Nastri E, Simoncelli M, Stochino F, et al. Resonance of steel wind turbines: problems and solutions. Structure. 2021;32:65–75.
28. Gao QF, Dong H, Deng ZW, Ma YY. Wind-induced dynamic amplification effects on the shallow foundation of a horizontal-axis wind turbine. Comput Geotech. 2017;88:9–17.

29. Harte M, Basu B, Nielsen S. Dynamic analysis of wind turbines including soil–structure interaction. Eng Struct. 2012;45:509–18.
30. Taddei F, Butenweg C, Klinkel S. Parametric investigation of the soil–structure interaction effects on the dynamic behaviour of a shallow foundation supported wind turbine considering a layered soil. Wind Energy. 2015;18:399–417.
31. Prowell I, Veletzos M, Elgamal A, Restrepo J. Experimental and numerical seismic response of a 65 kW wind turbine. J Earthq Eng. 2009;13(8):1172–90.
32. Bazeos N, Hatzigeorgiou G, Hondros I, Karamaneas H, Karabalis D, Beskos D. Static, seismic and stability analyses of a prototype wind turbine steel tower. Eng Struct. 2002;24: 1015–25.
33. Austin S, Jerath S. Effect of soil-foundation-structure interaction on the seismic response of wind turbines. Ain Shams Eng J. 2017;8:323–31.
34. Díaz O, Suárez LE. Seismic analysis of wind turbines. Earthq Spectra. 2014;30(2):743–65.
35. Nuta E, Christopoulos C, Packer JA. Methodology for seismic risk assessment for tubular steel wind turbine towers: application to Canadian seismic environment. Can J Civ Eng. 2011;38:293–304.
36. Dal Lago B, Flessati L, Marveggio P, Martinelli P, Fraraccio G, di Prisco C, et al. Experimental behaviour of shallow foundations of wind towers. Proceedings of the Italian concrete days. Milan, Italy; Collegio dei Tecnici per l'Industrializzazione Edilizia (CTE); 2020.
37. di Prisco M, di Prisco C, Fraraccio G, Colombo M, Dal Lago B, Flessati L, et al. Wind tower FRC foundations: research and design. Fibre reinforced concrete: improvements and innovations II. Cham, Switzerland: Springer International Publishing; 2022. https://doi.org/10.1007/978-3-030-83719-8_71
38. Martinelli P, Dal Lago B, Flessati L, Fraraccio G, di Prisco C, di Prisco M. Numerical analyses of shallow foundations of wind towers. Proceedings of the Italian concrete days. Milan, Italy; Collegio dei Tecnici per l'Industrializzazione Edilizia (CTE); 2020.
39. Harris HG, Sabnis GM. Structural modeling and experimental techniques. Boca Raton, FL: CRC Press; 1999.
40. EN 14651/2004. Test method for metallic fibered concrete: measuring the flexural tensile strength (limit of proportionality [LOP], residual). Brussels, Belgium; Comité européen de normalisation; 2004.
41. fib: fib Model Code for Concrete Structures 2010. fib Model Code for Concrete Structures 2010. Lausanne, Switzerland; Ernst & Sohn, Wiley; 2013.
42. di Prisco C, Imposimato S. Time dependent mechanical behaviour of loose sands. Mech Cohes-Frict Mater. 1996; 1(1):45–73.
43. Poulos HG, Davis EH. Elastic solutions for soil and rock mechanics. New York, USA: Wiley; 1974.
44. Meyerhof GG. The bearing capacity of foundations under eccentric and inclined loads. Proceedings of the 3rd international conference on soil mechanics and foundation engineering. Volume 1. Zurich, Switzerland: ICOSOMEF; 1953. p. 440–5.
45. Negro P, Paolucci R, Pedretti S, Faccioli E. Large scale soil-structure interaction experiments on sand under cyclic loading. Proceedings of the 12th world conference on earthquake engineering. Upper Hutt, New Zealand: New Zealand Society for Earthquake Engineering; 2000 1191.
46. di Prisco C, Nova R, Lanier J. A mixed isotropic-kinematic hardening constitutive law for sand. Mod Approach Plast. Amsterdam, Netherlands: Elsevier Science Publishers B.V.; 1993, pp. 83–124.
47. Martinelli P, Flessati L, Dal Lago B, Fraraccio G, di Prisco C, di Prisco M. Role of numerical modelling choices on the structural response of onshore wind turbine shallow foundations. Structure. 2022;37:442–458. https://doi.org/10.1016/j.istruc.2022.01.002

AUTHOR BIOGRAPHIES

Bruno Dal Lago, Assistant Professor, Department of Theoretical and Applied Sciences, Università degli Studi dell'Insubria, Varese, Italy.
bruno.dallago@uninsubria.it

Luca Flessati, Assistant Professor, Department of Civil and Environmental Engineering, Politecnico di Milano, Milan, Italy.
luca.flessati@polimi.it

Pietro Marveggio, Ph.D. Student, Department of Civil and Environmental Engineering, Politecnico di Milano, Milan, Italy.
pietro.marveggio@polimi.it

Paolo Martinelli, Assistant Professor; Department of Civil and Environmental Engineering, Politecnico di Milano, Milan, Italy.
paolo.martinelli@polimi.it

Giancarlo Fraraccio, Professional Engineer, Enel Green Power, Engineering and Construction Unit, Rome, Italy.
giancarlo.fraraccio@enel.com

Marco di Prisco, Professor, Department of Civil and Environmental Engineering, Politecnico di Milano, Milan, Italy.
marco.diprisco@polimi.it

Claudio di Prisco, Professor, Department of Civil and Environmental Engineering, Politecnico di Milano, Milan, Italy.
claudio.diprisco@polimi.it

How to cite this article: Lago BD, Flessati L, Marveggio P, Martinelli P, Fraraccio G, di Prisco C, et al. Experimental tests on shallow foundations of onshore wind turbine towers. Structural Concrete. 2022;1–21. https://doi.org/10.1002/suco.202100655